Perimeter Model for the Magnetic Circular Dichroism Spectrum of Deoxy Ferrous Heme in Myoglobin

Stefan Franzen*

Department of Chemistry, North Carolina State University, Raleigh, North Carolina 27695

Received: February 7, 2002; In Final Form: May 27, 2002

The magnetic circular dichroism (MCD) spectra of deoxy heme in Sperm whale myoglobin are explained by using a theory based on the perimeter model (PM) of metalloporphyrin spectra. The perimeter model is shown to be valid by comparison with the heme of carbonmonoxy myoglobin and previous reports including both Zn protoporphyrin and ferric heme MCD spectra. The PM approach, applied to closed shell metalloporphyrins, models the highest occupied molecular orbital as $L_z = \pm 4$ and the lowest unoccupied molecular orbital as $L_z = \pm 5$. According to the PM, the allowed intense Soret band transition has $L_z = \pm 1$, while the vibronically allowed weak Q-band has $L_z = \pm 9$.[1] Analysis of the experimental spectra based on the scaled first derivative of the absorption spectrum is demonstrated to give good agreement with calculated spectra, although the experimentally measured values of L_z are somewhat smaller than those predicted by the PM theory. Application of the PM to open shell metals, and in particular deoxy heme, is shown using a vibronic approach that accounts for mixing of charge-transfer states. A Soret excited-state split due to vibronic coupling (VC) is modeled by a porphyrin π excited state ($L_z = \pm 5$) that strongly vibronically couples with a dπ state ($L_z = \pm 1$). The vibronic coupling model has relevance not only for deoxy heme but also for species such as the heme oxo species known as compound I.[2] The model developed for MCD spectra is consistent with recent resonant Raman spectroscopic studies of deoxy heme.

Introduction

The heme in deoxy heme proteins is one of the most studied chromophores in the biophysical literature. The deoxy photoproduct of myoglobin, hemoglobin, and other heme proteins has been studied for over 50 years as an indicator of the conformational state of the protein following flash photolysis of ligands bound to the heme iron.[3−6] The interpretation of a large number of experiments on the dynamics of heme proteins rests on the assignments of the $\pi-\pi^*$ and charge-transfer electronic transitions of deoxy heme.[7,8] The interpretation of experimental band shifts in terms of protein structure has relied on the spectroscopic assignments and our understanding of the electronic and steric factors that affect the heme. This information is all the more interesting given the large amount of structural data from mutant X-ray crystal structures[9,10] and X-ray structures of photolyzed intermediates.[11−13] Despite this extensive study, the nature of the excited states of the deoxy heme chromophore has not yet been adequately addressed. A recent study of the resonant Raman spectra of the Q-band and charge transfer band III of deoxy heme indicates that both are vibronically coupled to the Soret band.[14] These results have bearing on the interpretation of spectroscopic data, including time-resolved band shifts of band III, the Soret band, and kinetic hole burning that have formed an underpinning for theories of protein dynamics.[15−21,9]

The magnetic circular dichroism (MCD) spectrum of deoxy heme has been studied, but there is still no conclusive interpretation of the anomalous negative first derivative signal for the Soret band. Magnetic circular dichroism spectroscopy gives information on the degeneracy of states and their splitting by geometric distortions due to vibronic coupling.[1] A spin−orbit coupling model was developed that fits the Soret band MCD data.[22,23] However, it was not applied to the Q-band, where the effects should have been at least as large given that the orbital angular momentum change is more than 5 times larger for the Q-band than for the Soret band.[24] A quantum chemical calculation including extensive configuration interaction (CI) has been applied to the deoxy heme MCD spectrum.[5,13,25] The conclusion of the authors includes spin−orbit interactions and the quintet states of high-spin heme iron with inclusion of CI from 28 excited-state configurations. The number of configurations precludes a simple interpretation of experimental data. Moreover, vibronic coupling has not been included in any of the previous studies of deoxy heme MCD data.

The perimeter model (PM)[26−28] shown in Figure 1 predicts that $\Delta L_z \approx 9$ for the Q-band, while $\Delta L_z \approx 1$ for the Soret band.[1,29] The nodal structure of the π-electrons is well represented by the wave functions obtained by a particle on a circle.[30] The PM is in approximate agreement with the MCD spectra of closed-shell metalloporphyrins.[24,31,32] The ferrous-CO adduct of myoglobin has no charge transfer states because of the low-spin electron configuration of the iron $(d_{xy})^2(d_{xz})^2(d_{yz})^2(d_{x^2-y^2})^0(d_{z^2})^0$. The quenching of angular momentum in open shell ferric hemes has been addressed though no specific coupling mechanisms were introduced.[33,34] The models for ferric heme have not been applied to deoxy heme. The open-shell configuration of high-spin ($S = 2$) deoxy heme, $(d_{xz})^2(d_{xy})^1(d_{yz})^1(d_{z^2})^1(d_{x^2-y^2})^1$, allows charge-transfer bands such as band III, which is a $a_{2u} \rightarrow d_{yz}$ ring-to-iron charge-transfer band. The extension of the PM to the open-shell deoxy heme requires consideration of vibronic coupling.

Vibronic coupling is key to an understanding of metalloporphyrin spectra. The four-orbital model accounts for configuration interaction of $a_{1u}(\pi) \rightarrow e_g(\pi^*)$ and $a_{2u}(\pi) \rightarrow e_g(\pi^*)$ transitions

* Corresponding author. Phone: (919)-515-8915. E-mail: Stefan_Franzen@ncsu.edu.

10.1021/jp025616k CCC: $22.00
Published on Web 00/00/0000 PAGE EST: 9.7

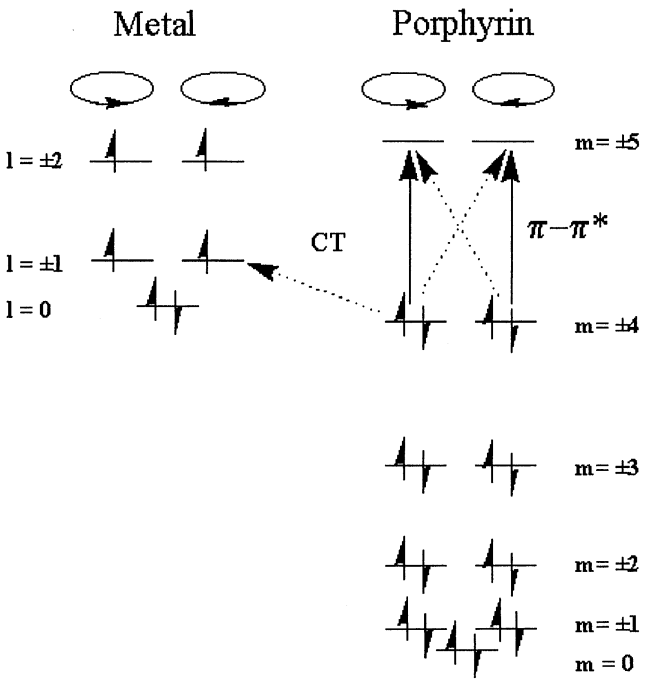

Figure 1. Energy level diagram for the circular perimeter model. The energy levels for the iron are included. The identification of the d-orbitals with particular angular momentum states is $L_z = 0$ for d_{z^2}, $L_z = 1$ for d_π, and $L_z = 2$ for d_{xy} and $d_{x^2-y^2}$.

that leads to a strongly allowed Soret band and much less intense Q-band, both with E_u excited-state configurations. Moreover, the E_u configuration the $a_{2u} \rightarrow d\pi$ charge-transfer states can mix with the E_u $\pi-\pi^*$ configurations by CI due to their identical symmetry. The direct product of two E_u electronic configurations yields four irreducible representations: $A_{1g} + A_{2g} + B_{1g} + B_{2g}$. The Soret band is Franck−Condon allowed and is mainly coupled to totally symmetric A_{1g} modes. The Q-band and band III both gain intensity through vibronic coupling (VC) that involves non-totally-symmetric modes of A_{2g}, B_{1g}, and B_{2g} symmetry. Since the zeroth-order E_u configurations are doubly degenerate, VC can occur by both intrastate Jahn−Teller (J−T) and interstate Herzberg−Teller (H−T) mechanisms.[35] The Q-band is coupled to the Soret band through H−T coupling by high-frequency modes that distort the periphery of the porphyrin ring. Vibronic mixing of this band principally involves the carbon atoms of the ring. The vibronic modes that give rise to this mixing are well-known from metalloporphyrin resonance Raman spectra. In deoxy heme the vibronic modes are ν_{10} (1610 cm^{-1}), ν_{11} (1546 cm^{-1}), and ν_{13} (1211 cm^{-1}) of B_{1g} symmetry,[36−39] as well as mode ν_{19} (1562 cm^{-1}) of A_{2g} symmetry.[40] The vibronic mixing of a charge-transfer transition with the Soret band involves H−T coupling by iron−pyrrole−nitrogen (Fe−Np) vibrations that are much lower in frequency. A 150-cm^{-1} mode that comprises a rhombic distortion associated with a low-frequency B_{1g} mode is strongly coupled to both the Soret band and charge-transfer band III in deoxy heme.[14] The frequency of the 160-cm^{-1} mode observed in the resonant Raman spectra of band III at 40 K in ref 14 corresponds to the 150-cm^{-1} mode observed in the room-temperature Soret resonant Raman spectrum. The temperature-dependent frequency shift of the 150 cm^{-1} mode due to anharmonic coupling is similar in magnitude to that of the Fe−His mode, which shifts from 218 to 228 cm^{-1} over the same temperature range.[41] It will be shown in the following that incorporation of vibronic coupling into the PM leads to a theory for the A_1, B_0, and C_0 terms observed experimentally for the deoxy heme Q-band, band III, and Soret band, respectively.[8,42,43] The treatment here preserves the simplicity of the PM and yet contains the essential features of the different both J−T and H−T VC mechanisms. Although this study focuses on ferrous deoxy heme, the simple model presented here is general and can be combined with a previous approach[33,34] to angular momentum quenching to address a general interpretation of MCD signatures in hemes.

Experimental Section

Sperm whale myoglobin was obtained from *E. Coli* by previous published procedures. Samples were handled at 4 °C in 100 mM potassium phosphate buffer pH 7.4 unless otherwise stated. Heme protein concentrations were determined by the pyridine hemochromogen method.[44]

UV−visible absorption spectra were recorded with a Cary 210 spectrophotometer interfaced to an IBM PC. MCD spectra were measured at 4 °C using a JASCO J500-A spectropolarimeter equipped with a JASCO MCD-1B electromagnet (1.41 T) and interfaced to a Gateway 2000 4DX2-66V PC through a JASCO IF-500-2 interface unit as previously described.[45]

Methods

The Perimeter Model. The free electron model (FEM) was applied to metalloporphyrins more than 50 years ago and provides a simple means of quantitatively interpreting the MCD spectra of metalloporphyrins.[26−28] The FEM approach is important because of the difficulty of calculating the orbital angular momentum from first principles. In the present study we consider the wave functions of the FEM as the basis functions in a PM that includes both porphyrin ring and metal orbital angular momenta (Figure 1). The wave functions,

$$\Phi_{\pm} = \frac{1}{\sqrt{2\pi}} e^{\pm im\phi} \tag{1}$$

($m = 0, \pm1, \pm2$, etc.) are obtained by solving the Schrödinger equation for an electron traveling in a circular orbit,

$$-\frac{h^2}{2meR_0{}^2}\frac{\partial^2}{\partial\phi^2}\Phi = E\Phi \tag{2}$$

where m_e is the mass of the electron and R_o is the radius of the circle. The quantum numbers m represent the orbital angular momenta of the electrons in particular orbitals.[31,32,46] The energy levels shown in Figure 1 are

$$E = \frac{h^2m^2}{2m_eR_0{}^2} \tag{3}$$

As shown in Figure 1, there are 18 π-electrons in the aromatic metalloporphyrin ring leading to the prediction that the levels $m = \pm4$ are the highest occupied molecular orbitals and the levels $n = \pm5$ are the lowest unoccupied molecular orbitals. In the following, m and n refer to ground- and excited-state quantum numbers, respectively. The angular momentum change is $\Delta L_z = n - m$. There are two possible transitions with angular momentum changes or $\Delta L_z = \pm1$ from $4 \rightarrow 5$ and $-4 \rightarrow -5$ or $\Delta L_z = \pm9$ from $4 \rightarrow -5$ and $-4 \rightarrow 5$. The prediction that the orbital angular moment quantum number is $\Delta L_z = 1$ for the strongly allowed Soret band and $\Delta L_z = 9$ for the Q-band follows from this simple model. It has been shown that this approach can be used to model the A_1 term of MCD spectra, since that term is directly proportional to the orbital angular momentum ΔL_z. The perimeter model used here is not valid

for states higher than $n = \pm 5$, since it predicts that the orbital angular momentum will increase without bound in contradiction to experiment. This potential shortcoming of the model does not affect the results, since higher metalloporphyrin transitions (e.g., the N-band) are not considered here.

The perimeter model also includes the orbital angular momenta of the iron as shown in Figure 1. Following the treatment of Koboyashi for ferric hemes, the d-electrons contribute to the orbital angular momentum as follows:[33,34]

$$d_{z^2} \qquad L_z = 0$$

$$d_{xz}, d_{xz} \qquad L_z = \pm 1$$

$$d_{xy}, d_{x^2-y^2} \qquad L_z = \pm 2$$

Thus, the relevant angular term of the iron wave functions have the form of eq 1. In other words, we consider only the azimuthal part of the iron d-orbitals as relevant for determining the contribution to L_z.

The terms in MCD are denoted A_1, B_0, and C_0 as indicated in eq 4.

$$\Delta A(\nu) = A_1\left(-\frac{\partial f(\nu)}{\partial \nu}\right) + \left(B_0 + \frac{C_0}{k_B T}\right) f(\nu) \qquad (4)$$

Equation 4 suggests that by simply comparing the negative of the first derivative of the line shape it should be possible to determine the A_1 parameter, which leads directly to an estimate of the angular moment change for the transition.

A relatively simple MO approach to the MCD spectra of ferric hemes ($S = 1/2$, 3/2, and 5/2) was developed by Koboyashi[33] (see also Supporting Information). For ferric hemes the theory addresses the quenching of orbital angular momentum by charge-transfer states that leads to a smaller MCD signal than that seen in the closed-shell poprhyrins. However, this approach has not been generally applied to open-shell metals. For example, deoxy heme has not been examined by using these models. Deoxy heme in myoglobin is observed in a high-spin state ($S = 2$) at room temperature with a d-electron configuration of $(d_{xz})^2(d_{xy})^1(d_{yz})^1(d_{x^2-y^2})^1(d_{z^2})^1$. The ordering of the electron states in the study of Eaton et al. is consistent with the B_0 term MCD signal for the $a_{2u} \rightarrow d_{yz}$ charge-transfer band of deoxy heme (band III) reported in their study.[8] Mixing of charge-transfer bands with the allowed $\pi-\pi^*$ transitions has been suggested for deoxy heme; however, the orbital angular momentum quenching that is evident in $Fe^{III}H_2O$ (metaquo) hemes does not appear to occur. Instead the MCD signal of the Soret band of deoxy heme is actually larger than that of the closed-shell CO-heme and reversed in sign. Moreover, the deoxy Mb Q-band MCD signal is of nearly the same magnitude as the closed-shell MbCO MCD signal, a fact that has not been widely appreciated due to the fact that the first derivative comparisons have not been used to aid in the visualization.

Extraction of the MCD Parameters. The extraction of MCD parameters A_1, B_0, and C_0 has been discussed by Piepho and Schatz[47] using the method of moments (MM). The MM has limited utility for spectra with overlapping bands. The MM requires integration over an entire band to obtain the dipole strength D_0 and the MCD parameters, A_1, B_0, and C_0. As a consequence, the average value of the MCD parameter will be obtained if more than one transition or vibronic band is present. The MM approach is problematic for heme since there are numerous vibronic bands where orbital angular momentum quenching may reduce the magnitude of A_1 in the $0-n$ vibronic satellite bands relative to the $0-0$ band (see Supporting Information). The details of the application of these methods to the data for deoxy and carbonmonoxy ferrous hemes are described in detail in the Supporting Information where fits to the data and the details of numerical analysis are presented.

TABLE 1: Comparison of the Experimentally Determined ΔL_z for the Various Methods[a]

species	MM	SFD	MG-SFD
MbCO Q	4.76 ± 0.44	5.14 ± 0.16	7.28 ± 0.24
MbCO Soret	0.72 ± 0.10	1.00 ± 0.04	0.88 ± 0.04
deoxy Mb Q	5.18 ± 0.80	4.28 ± 0.16	6.58 ± 0.64
deoxy Mb Soret	-2.12 ± 0.44	-3.84 ± 0.12	-2.98 ± 0.16

[a] The orbital angular moment is proportional to the ratio of the A_1 parameter to the dipole strength D_0. The details of how these parameters were obtained are discussed in detail in the Supporting Information.

An alternative approach based on scaled first derivatives (SFD) of the absorption spectrum is applicable to the fitting of A_1, B_0, and C_0 parameters relevant to the MCD spectra of heme. If the absorption spectrum has multiple bands, the scaling of the entire absorption spectrum suffers from the same deficiency as the MM approach outlined above. An extension of the SFD approach involves fitting the absorption spectrum to a number of Gaussian functions and then a subsequent scaling of the first derivatives of each Gaussian independently to fit the MCD spectrum. The multiple Gaussian scaled first derivative (MG-SFD) approach permits different A_1, B_0, and C_0 parameters for the vibronic bands. Each of these approaches is presented in the Supporting Information, including figures that show the fits. The details of the MG-SFD approach are given below. The results of the fits are given in Table 1. The philosophy of the MG-SFD approach is similar to that used extensively in Stark effect spectroscopy.[48−51] In the Stark effect, the various electric-field-dependent terms are manifested as the zero, first, and second derivative of the absorption spectrum. The analysis of these derivatives is based on a rigid shift treatment of the absorption band developed by Liptay.[48] In the limit of small shifts, this method is implemented by fitting to the derivatives. In practice, the absorption line shape is fit to a number of Gaussian functions whose derivatives are then scaled collectively to match the electric-field-modulated difference spectrum, $\Delta\epsilon(F,\nu)$.[50] The change in the extinction coefficient arises from the interaction of the electric field with the difference dipole moment, $\Delta\mu_A$, and the difference polarizability, $\Delta\alpha$. The innovation presented in this work applies the same analysis to magnetic field modulated spectra, $\Delta\epsilon(H,\nu)$. Based on the work of Piepho and Schatz[47] the ratio of the derivative of the line shape, $\partial\phi(\nu)/\partial\nu$, and the line shape function itself, $\phi(\nu)$, yields yields a direct estimate for the change in angular momentum, ΔL_z. In tetragonal symmetry, e.g., D_4, C_{4v} or D_{4h}, we obtain

$$\frac{\Delta\epsilon_m(\nu)}{\epsilon(\nu)} = \frac{A_1\mu_B}{D_0}\frac{\left(-\frac{\partial f(\nu)}{\partial \nu}\right)}{f(\nu)} \qquad (5)$$

$$\Delta L_z = 2\frac{A_1}{D_0} \qquad (6)$$

The factor of 2 in eq 6 arises from symmetry considerations in a molecule with tetragonal symmetry as discussed in Chapter 17 of Piepho and Schatz.[47] Equation 6 indicates that a change in angular momentum is required to observe the MCD signal. The hypothesis of this study is that the orbital angular momentum of the metalloporphyrin is the dominant contribution.

TABLE 2: Gaussian Fitting Parameters for the Soret- and Q-Band Absorption Spectra and First Derivative Models of Magnetic Circular Dichroism

α_n	ν_0	s	$\beta = -(\partial f(\nu)/\partial\nu)/f(\nu)$
	Carbonmonoxy Soret Band		
$(1.87 \pm 0.2) \times 10^7$	23634 ± 2	197 ± 6	0.206 ± 0.01
$(9.52 \pm 0.09) \times 10^7$	23661 ± 7	356 ± 23	0.250 ± 0.005
$(1.21 \pm 0.02) \times 10^8$	24230 ± 1	1083 ± 4	0.171 ± 0.01
$(3.34 \pm 0.09) \times 10^7$	21500 (fixed)	2500 (fixed)	3.81 ± 0.22
	Carbonmonoxy Q-Band		
$(3.323 \pm 0.12) \times 10^6$	17250 ± 5	172 ± 3	1.701 ± 0.06
$(1.940 \pm 0.12) \times 10^6$	17615 ± 11	191 ± 7	1.406 ± 0.13
$(4.907 \pm 0.28) \times 10^6$	18455 ± 43	345 ± 22	0.980 ± 0.13
$(2.182 \pm 0.022) \times 10^7$	18620 ± 16	1047 ± 15	0.250 ± 0.19
	Deoxy Soret Band		
$(3.88 \pm 0.07) \times 10^7$	22815 ± 3	316 ± 1	0.528 ± 0.02
$(2.67 \pm 0.07) \times 10^7$	23279 ± 7	350 ± 2	-0.699 ± 0.04
$(9.99 \pm 0.05) \times 10^7$	23744 ± 2	786 ± 2	-0.191 ± 0.005
$(2.47 \pm 0.01) \times 10^8$	26060 ± 26	2444 ± 12	0.005 ± 0.001
	Deoxy Q-Band		
$(1.08 \pm 0.09) \times 10^6$	17050 ± 14	282 ± 11	2.006 ± 0.16
$(7.61 \pm 0.24) \times 10^6$	17862 ± 10	533 ± 11	1.036 ± 0.06
$(3.60 \pm 0.01) \times 10^7$	18839 ± 12	1694 ± 12	0.178 ± 0.09

The contribution of a spin−orbit interaction is not precluded by the present model, but it is not explored here.

Multiple Gaussian Scaled First Derivative Approach. The absorption line shape and MCD spectrum can be fit to a number of Gaussian functions that may correspond to vibronic bands. The line shape function is defined in eq 7 as

$$A(\nu) = f(\nu) = \sum_{n=1}^{N} \frac{\alpha_n}{\sqrt{2\pi}\sigma_n} \exp\left\{-\frac{(\nu - \nu_n)^2}{2\sigma_n^2}\right\} \quad (7)$$

Each Gaussian function has an amplitude α_n, variance σ_n and position ν_n. These parameters are given in Table 2 for the data discussed below. The A_1 term MCD spectrum was then modeled by using the fitted line shape function with no adjustment other than a scaling parameter β.

$$\Delta A(\nu) = \beta\frac{\partial f(\nu)}{\partial \nu} = \beta\sum_{n=1}^{N} -(\nu - \nu_n)\frac{\alpha_n}{2\pi\sigma^3 n} \exp\left\{-\frac{(\nu - \nu_n)^2}{2\sigma^2 n}\right\} \quad (8)$$

The MCD signal for vibronic bands can vary depending on the nature of vibronic coupling. An example for the excited state is indicated above. Ground-state splitting can be modeled in a similar fashion. When this occurs the parameter β can be distributed among the various Gaussian components as β_n:

$$\Delta A(\nu) = \sum_{n=1}^{N} \beta_n \frac{\partial f_n(\nu)}{\partial \nu} = \sum_{n=1}^{N} -(\nu - \nu_n)\frac{\beta_n\alpha_n}{\sqrt{2\pi}\sigma_n^3} \exp\left\{-\frac{(\nu - \nu_n)^2}{2\sigma^2 n}\right\} \quad (9)$$

It may seem redundant to have two parameters, α_n and β_n. However, the method used fixes α_n according to the fit to the absorption spectrum. Thus, the relative magnitude of vibronic terms is easily identified using β_n. For the nth vibronic band $\beta_n = \mu_B A_1/D_0$, where the A_1 parameter corresponds exclusively to the nth band. The C_0-term MCD signal is calculated by using Gaussian fit parameters. In fitting the data the parameters for the four-Gaussian fit to the Soret band were kept constant and a shifted and scaled line-shape function was allowed to adjust to the MCD data. The C_0-term model is

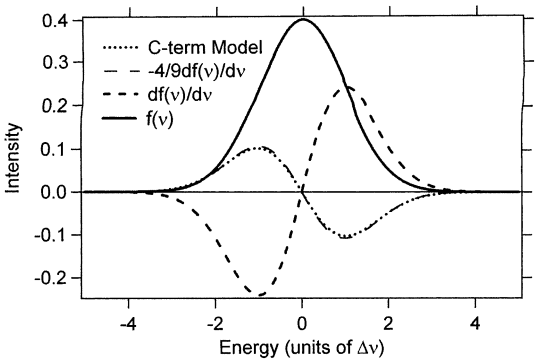

Figure 2. Sample spectra calculated for a single Gaussian. The spectra are plotted in units of the variance. The figure compares explicit calculation of the C_0-term by using shifted Gaussian with the first derivative of a Gaussian. The two approaches are shown to yield similar results for the magnitude of shift observed in typical MCD spectra.

$$\Delta A(\nu) = \gamma(f(\nu) - f(\nu - \nu_s)\} = \gamma\sum_{n=1}^{N} \frac{\alpha_n}{\sqrt{2\pi}\sigma_n}\left(\exp\left\{-\frac{(\nu - \nu_n)^2}{2\sigma^2 n}\right\} - \exp\left\{-\frac{(\nu - \nu_n - \nu_s)^2}{2\sigma^2 n}\right\}\right) \quad (10)$$

A sample calculation using a single Gaussian is shown in Figure 2. The derivative of the Gaussian line shape shown in Figure 2 serves as a model of the A_1-term MCD signal. Figure 2 also shows that the inverted first derivative line shape has a similar shape to the shifted Gaussian model for small values of the shift parameter ν_s in eq 10. To model the C_0-term MCD signal we need to estimate the relationship between the bandwidth $\Delta\nu$, the excited-state splitting energy ΔE, and thermal energy kT. For the deoxy Soret band model, the homogeneous line width is $\Delta\nu \approx 300$ cm^{-1} and $kT \approx 200$ cm^{-1} (at 300 K). If $\Delta E/\Delta\nu \approx 1/3$ (i.e., $\Delta E \approx 100$ cm^{-1}), the line shape of the C_0 term has the form of a first derivative and the correct magnitude to model the experimental data. The comparison is indicated in Figure 2 where a Gaussian model and first derivative are compared. The point of this comparison is that it demonstrates the equivalence of an inverted A_1-parameter expression ($\alpha_n < 0$) using eq 9 and the C_0-term model given by eq 10 for fitting a model of the deoxy Soret band.

Results

The data shown in Figures 3−6 are the absorption and MCD spectra of MbCO and deoxy Mb, respectively. The dashed lines in Figures 3A−6A are Gaussian fits to the absorption spectra and those in Figures 3B−6B represent the scaled first derivatives of the Gaussian functions (MG-SFD) of the absorption spectra scaled to match the magnitude of the corresponding MCD spectra. The Gaussian fitting parameters and scaling coefficients for the MG-SFD approach that result from the fits to the data are given in the Table 2. The choice of the first derivative arises from the form of MCD predicted by theory. The scaling factor used to obtain agreement with the MCD signal is proportional to the ratio of the A_1 parameter to the dipole strength, D_0. The ratio A_1/D_0, in turn, is proportional to the change in orbital

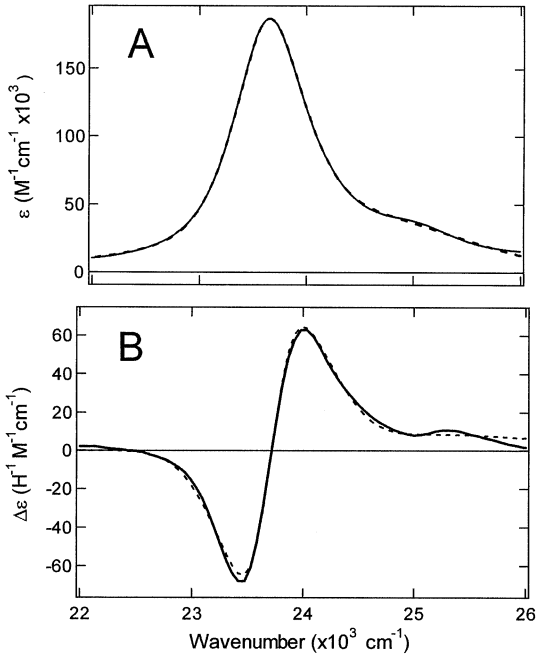

Figure 3. (A) Absorption spectrum for the Soret band of carbonmonoxy heme in myoglobin. The line shape was determined by the fit to four Gaussians. The parameters for the fits are given in Table 2. (B) Magnetic circular dichroism spectrum for the Soret band of carbonmonoxy heme. The MCD signal was modeled as a scaled first derivative (MG-SFD) as given by eq 9. The scaling factors β_n are given in Table 2.

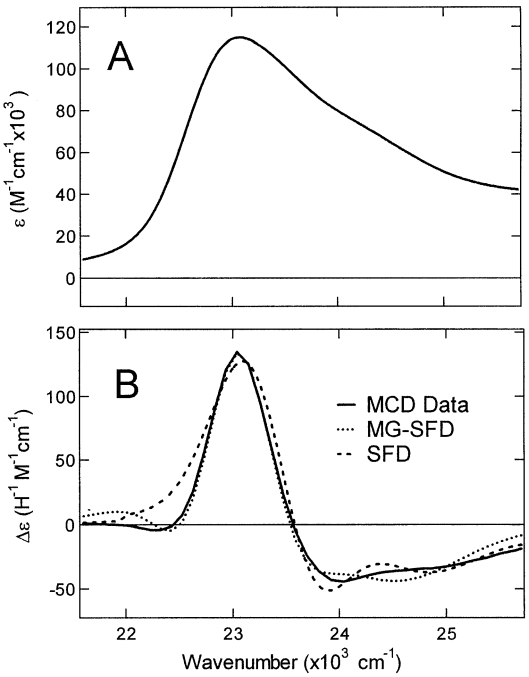

Figure 5. (A) Absorption spectrum for the Soret band of deoxy heme in myoglobin. (B) Magnetic circular dichroism spectrum for the Soret band of deoxy heme. The data were fit both with a multiple Gaussian scaled first derivative (MG-SFD) and a SFD approach without individual vibronic bands.

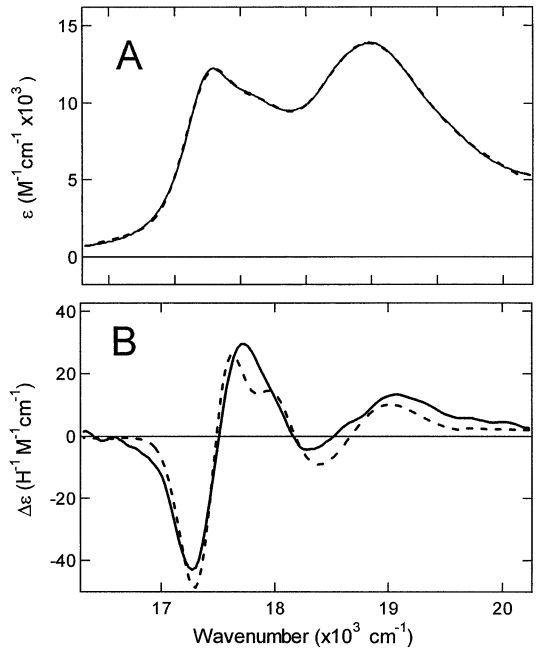

Figure 4. (A) Absorption spectrum for the Q-band of carbonmonoxy heme in myoglobin. (B) Magnetic circular dichroism spectrum for the Q-band of carbonmonoxy heme. The MCD signal was modeled as a scaled first derivative (MG-SFD) as given by eq 9. The scaling factor β for the MG-SFD fit given in Table 1 is more than 8 times larger than the found for the Soret band of heme-CO shown in Figure 1B.

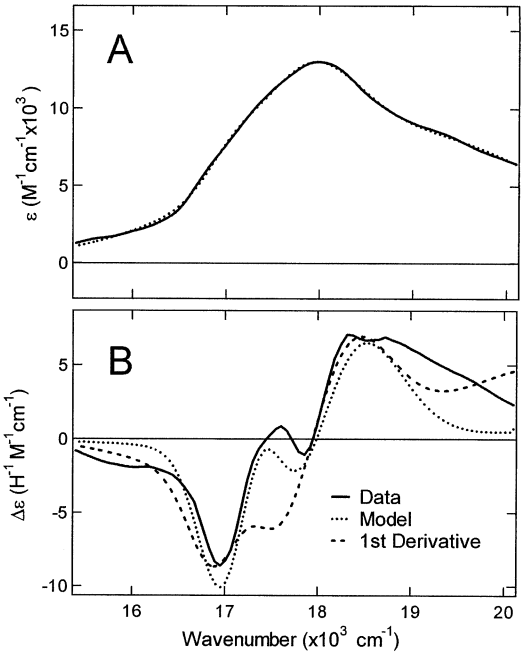

Figure 6. (A) Absorption spectrum for the Q-band of deoxy heme in myoglobin. (B) Magnetic circular dichroism spectrum for the Q-band of deoxy heme. The MG-SFD approach (eq 9) was used to account to model the quenching of MCD signal strength in the 0−1 (dotted line in Figure 5B).

angular momentum, ΔL_z for the electronic transition. The calculated values for ΔL_z are presented for four methods in Table 1. In contrast to the MG-SFD method, the SFD method was implemented by taking the numerical derivative of the absorption spectrum followed by application of a scaling factor. The SFD model is quite adequate for the Soret band region of heme-CO. However, the model yields a poorer fit to the data in the Q-band region, particularly in the vibronic bands. The fits for the deoxy Soret band and Q-band MCD spectra are different than that for the CO adduct in that the sign of the first derivative term required is negative and the magnitude is about 4 times as large as for the CO heme Soret band (Table 2). Although the negative first derivative signal can be modeled by using the

MG-SFD approach, the signal seen in Figure 5B is indicative of C_0-term MCD. The Q-band deoxy heme MCD spectrum can be reasonably modeled by a first-derivative approach. However, the vibronic 0−1 (middle band) is much smaller in the MCD spectrum than in the MG-SFD. The smaller 0−1 band can be understood from the fact that VC in the Q-band region results in orbital angular momentum quenching in the Q-band. The model calculation for VC includes separate parameters for the derivative representing the 0−0 and 0−1 bands as discussed below.

Calculation of the A_1 Parameter MCD Signal by Using the Perimeter Model (PM). In the perimeter model, the A_1-term MCD signal where both degenerate excited states and ground states are present is given as

$$A_1 = \frac{1}{2}(\langle E_\pm|L_z|E_\pm\rangle - \langle G_\pm|L_z|G_\pm\rangle) \times (\langle E_\pm|\mu_{-1}|G\pm\rangle^2 - \langle E_\pm|\mu_{+1}|G_\pm\rangle^2) \quad (11)$$

where μ represents the dipole operator. Substituting in one sign from the perimeter wave functions and the orbital angular momentum operator we have

$$A_1 = \frac{1}{2}\left(\left\langle e^{\pm in\phi}\right|-i\frac{\partial}{\partial\phi}\left|e^{\pm in\phi}\right\rangle - \left\langle e^{\pm im\phi}\right|-i\frac{\partial}{\partial\phi}\left|e^{\pm im\phi}\right\rangle\right) \times (\langle e^{\pm in\phi}|e^{-i\phi}|e^{\pm im\phi}\rangle^2 - \langle e^{\pm im\phi}|e^{+i\phi}|e^{\pm im\phi}\rangle^2) \quad (12)$$

The first two integrals give the angular momentum in the excited state (quantum number n) and in the ground state (quantum number m), respectively. The values of the excited-state and ground-state angular momenta are

$$\langle G_\pm|L_z|G_\pm\rangle = \frac{1}{2\pi}\left\langle e^{\pm im\phi}\right| - i\frac{\partial}{\partial\phi}\left|e^{\pm im\phi}\right\rangle = \pm m$$

$$\langle E_\pm|L_z|E_\pm\rangle = \frac{1}{2\pi}\left\langle e^{\pm in\phi}\right| -i\frac{\partial}{\partial\phi}\left|e^{\pm in\phi}\right\rangle = \pm n \quad (13)$$

The last two integrals in eq 12 are the transition moments for the Soret band or B-band, M_B, if $m = \pm 4$ and $n = \pm 5$:

$$\langle e^{\pm in\phi}|e^{\pm i\phi}|e^{\pm im\phi}\rangle = \frac{1}{2\pi}\int_0^{2\pi} e^{i(\mp n\pm m\pm 1)\phi}\,d\phi = \delta_{m\pm 1,n} \quad (14)$$

On the other hand, for $m = \pm 4$ and $n = -5$, eq 14 represents the transition moment for the Q-band, $M_Q = \langle G_\mp|\mu_\pm|E_\pm\rangle = 0$. The Q-band or CT-band transitions can gain intensity by vibronic coupling. In the following, the intensities will be discussed relative to $M_B = \langle G_\pm|\mu_\pm|E_\pm\rangle = 1$ as indicated by eq 14 for $n = m|$ when m and n have the same sign. Thus, $A_1 = |n - m|/2$ for the perimeter model for the Soret band of MbCO where the iron is low spin and there is no excited-state vibronic or Jahn−Teller splitting. The A_1 parameter for the Q-band is expected to be 9 times as large as that for the B-band, i.e., the $\Delta L_z = 9$ transition ($m = -4 \rightarrow n = 5$ and $m = 4 \rightarrow n = -5$),- which represents the Q-band. However, the $\Delta L_z = 9$ transition or Q-band transition gains intensity only in the presence of vibronic coupling as considered explicitly below.[46]

The A_1-parameter analysis applies to the MCD data for closed-shell metals where the excited state is doubly degenerate. In the presence of sufficiently large Herzberg−Teller (H−T) or Jahn−Teller (J−T) vibronic coupling the excited-state degeneracy is removed (see Supporting Information). The resulting splitting of the excited levels eliminates the A_1-parameter contribution to the MCD signal (eq 4). However, the ground-state angular momentum is unchanged and $\langle G_\pm|L_z|G_\pm\rangle = 4$. The PM A_1 term predicts that the magnitude of the MCD signal for the split Soret of deoxy Mb would be 4 times as large as the doubly degenerate Soret of MbCO and reversed in sign. Table 2 shows that this qualitative reasoning agrees quite well with the data shown in Figure 5. Figure 2 shows the similarity of an inverted A_1-parameter MCD signal and a C_0-parameter MCD signal when the ground state is the sole contribution to the orbital angular momentum. However, in a formal treatment, a doubly degenerate ground state gives rise to a temperature-dependent C_0-term MCD signal. Consistent with this expectation the MCD signal for the deoxy Soret band depends on temperature.[52] The derivation of the C_0-term MCD signal using a vibronic coupling PM is considered below. It is possible to consider a pseudo-B_0-term MCD signal that will arise from the split Soret excited state. However, it is shown below that the vibronic mixing of the Q-band and the Soret band will contribute less than 1/10 the oscillator strength of the Soret band itself and this effect is relatively small. The observed A_1-term MCD spectra for the deoxy Q-band and the Q and Soret bands of MbCO indicate that J−T and H−T vibronic coupling is sufficiently weak that the splitting of the excited state is negligible in the Q-band. This observation leads to consideration of the vibronic interaction of the deoxy Soret band and charge-transfer band III as an explanation for the differences between open- and closed-shell deoxy hemes.

Vibronic Coupling Perimeter Model VCPM. There are two categories of vibronic modes considered in this treatment of the MCD signal of metalloporphyrins. First, there are the modes that give rise to Q-band intensity. These interstate H−T active modes have been studied and the correct relative intensities have been determined.[46] There are also intrastate J−T active vibronic modes[53] that lead to a splitting of the excited state that are not accounted for by the theory of Perrin et al.[46] The vibronic model of Perrin et al. was particularly intended to explain the vibronic intensity of Q-band transitions in benzene and similar transitions in other in $4n + 2$ aromatic molecules, including metalloporphyrins. A similar result is derived below by using the perimeter model, showing the correspondence with previous work.[46] Neither the Perrin model nor the PM can explain excited-state splitting of metalloporphyrins unless the angular momentum of a central metal atom is included in the model. The VC model of interest for deoxy heme involves mixing of the dπ orbitals of the iron ($L_z = \pm 1$) with the $e_g\pi^*$ states of the ring ($L_z = \pm 5$) as shown in Figure 1 and described above in the Methods section.

The vibronic matrix elements can be modeled by assuming a geometry distortion of the circular π-electron system. Considering only radial distortions, the vibrational Schrödinger equation is

$$-\frac{\hbar^2}{2M}\left(\frac{\partial^2}{\partial R^2} + \frac{2}{R}\frac{\partial}{\partial R}\right)\Psi + \frac{1}{2}k(\phi,R_0)R^2\Psi = E\Psi \quad (15)$$

In the vibrational equation M represents the reduced mass of the nuclei in the ring and $k(\phi,R_0)$ represents a radial force constant in the crude adiabatic approximation. The nuclear equation of state permits a vibronic mode to couple two electronic states by distorting the molecular geometry. The geometry distortion in a LCAO model was introduced in the vibronic model of Perrin, Goutermann, and Perrin[46] by distortion of the ring from a circular shape by using discrete points around a circle that represented by the nuclei of the π-electron centers. In the current treatment the force constant depends on the electronic coordinate at a fixed radius R_0 of the PM. The radial

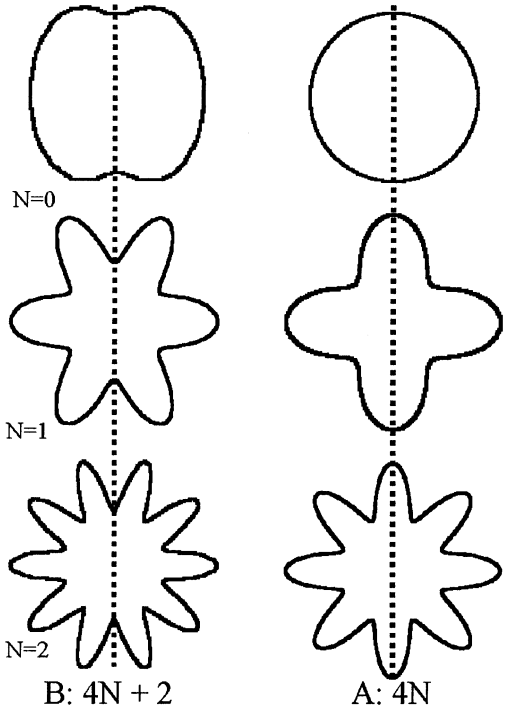

Figure 7. Form of the circular trajectory of an electron in the circular PM compared to a geometry distortion with a 4-fold symmetry axis. The possible modes are either B_{1g} or A_{2g} symmetry modes, which have vibrational quantum numbers $\nu = 4N + 2$ or $4N$, respectively, where $N = 0, 1, 2, ...$ These are shown on the right- and the left-hand side of the figure, respectively.

distortion can be approximated by using a parametric dependence of the force constant on the angle ϕ:

$$k(\phi,R_0) = k(R_0)\cos(\nu\phi) \tag{16}$$

where ν is the vibrational quantum number as shown in Figure 7. For example, a B_{1g} mode is modeled by $\cos(6\phi)$ such that the ring is distorted into the six-lobed shape shown in Figure 7. The VC operator is obtained from the expansion in terms of the radial coordinate:

$$V(R,\phi) = V(R_0,\phi) + \frac{\partial V(R_0,\phi)}{\partial R}\Delta R + \frac{\partial^2 V(R_0,\phi)}{\partial R^2}\Delta R^2 + ... \tag{17a}$$

where

$$\frac{\partial V}{\partial R}\Delta R = k(\phi,R_0)(R - R_0)\Delta R = k\Delta R^2\cos(\nu\phi) \tag{17b}$$

In the following we use $k = k(R_0)$ to simplify notation. Using this approximation for the vibronic operator of the PM, the VC matrix elements are

$$\frac{1}{2\pi}\left\langle E_-\left|\frac{\partial V}{\partial R}\right|CT_+\right\rangle\Delta R = \frac{k\Delta R^2}{2\pi}\langle e^{-i5\phi}|\cos(6\phi)|e^{i\phi}\rangle = -\frac{k\Delta R^2}{2}$$

$$\frac{1}{2\pi}\left\langle E_+\left|\frac{\partial V}{\partial R}\right|CT_-\right\rangle\Delta R = \frac{k\Delta R^2}{2\pi}\langle e^{i5\phi}|\cos(6\phi)|e^{-i\phi}\rangle = \frac{k\Delta R^2}{2} \tag{18}$$

The model predicts a vibronic splitting of the excited state of magnitude $k\Delta R^2$. The relationship between this harmonic energy and the vibronic mode energy is given by

$$\frac{k\Delta R^2}{2} = \langle\hbar\omega\rangle_{av} = \frac{\hbar\omega}{2} + (1 - e^{-\hbar\omega/k_BT})\sum_{\nu=1}^{\infty}\nu\hbar\omega e^{-\nu\hbar\omega/k_BT} \tag{19}$$

The average energy in the vibronic mode is given by the product of the vibrational partition function and the quantum mechanical level spacing as indicated on the right-hand side of eq 19. The expression takes into account the fact that a low-frequency mode will have significant population of vibrational levels with quantum number greater than $\nu = 1$. For a 150-cm^{-1} mode relevant to the discussion below, $\langle\hbar\omega\rangle_{av} \approx 175$ cm^{-1} at 300 K.

There are four possible transitions from the degenerate ground state to the split excited-state levels. The splitting of the excited state leads to a C_0-term MCD signal:

$$C_{0-} = -\frac{1}{2}(\langle G_-|L_z|G_-\rangle\langle E_-|\mu_{-1}|G_-\rangle^2 - \langle G_+|L_z|G_-\rangle\langle E_-|\mu{-}_1|G_+\rangle^2)$$

$$C_{0+} = -\frac{1}{2}(\langle G_+|L_z|G_+\rangle\langle E_+|\mu_1|G_+\rangle^2 - \langle G_-|L_z|G_-\rangle\langle E_+|\mu_1|G_-\rangle^2) \tag{20}$$

where the reversed sign for the transition moments in the C_{0+} term follows from the time-reversal operator as described in Chapter 14 of Pipeho and Schatz.[47] Two of the terms are zero, so that the only terms that contribute to the observed C_0-term MCD signal are obtained by substituting in the perimeter functions:

$$C_{0+} = \frac{m}{2}\frac{1}{4\pi^2}\langle e^{in\phi}|e^{i\phi}|e^{im\phi}\rangle^2 = \frac{m}{2}$$

$$C_0{-} = -\frac{m}{2}\frac{1}{4\pi^2}\langle e^{-in\phi}|e^{-i\phi}|e^{-im\phi}\rangle^2 = -\frac{m}{2} \tag{21}$$

This result obtained with zero-order perimeter wave functions for the ground electronic state is identical to that obtained using an A_1-term model with no excited-state angular momentum. The change in orbital angular momentum is $\Delta L_z = 2A_1/D_0$ (eq 6) and $2C_0/D_0$ for these two models, respectively, as discussed in more detail in the Supporting Information. The mathematical equivalence of these treatments is demonstrated in Figure 2. The treatment of the Soret band splitting follows interstate H−T coupling. In principle, the derivation above would need to be modified by the H−T perturbative term to account for the mixing of the wave functions of the dπ and $e_g\pi^*$ states. The H−T vibronic term is given by

$$|CT\rangle = |CT_\pm\rangle + \frac{\left\langle E_\mp\left|\frac{\partial V}{\partial R}\right|CT_\pm\right\rangle}{E_\mp - E_{CT}}\Delta R|E_\mp\rangle + ... \tag{22}$$

where $|CT\rangle$ represents the vibronically coupled charge transfer state and $|CT_\pm\rangle$ represents the zero-order basis state. The energy denominator, $\Delta E_{CT} = E_\mp - E_{CT}$, is given by the matrix elements of the respective states in the perimeter model in the Appendix or determined from experiment. The magnitude of the numerator of the perturbative term is $\langle\hbar\omega\rangle_{av}$ given by eqs 18 and 19. If we estimate $\langle\hbar\omega\rangle_{av} \approx 175$ cm^{-1} and $\Delta E_{CT} = E_{\pi^*} - E_{dyz} \approx 10\,000$ cm^{-1} from experiment, the vibronic correction to the wave function is $\langle\hbar\omega\rangle_{av}/\Delta E_{CT} \approx 0.02$. The experimental estimate for ΔE_{CT} is obtained from the difference between the Soret and band III energies in the absorption spectrum. The mixing

parameter, $\langle\hbar\omega\rangle_{av}/\Delta E_{CT}$ is sufficiently small to justify the use of the zero-order wave functions for the analysis of the C_0 term in eq 21.

The *B*-Term MCD of Charge-Transfer Band III. The incorporation of VC into the PM provides an explanation for the B_0-term MCD signal of charge-transfer band III. The CT band has been assigned as an $a_{2u} \rightarrow d_{yz}$ transition.[8] Assuming that both the ground and excited states are doubly degenerate in agreement with the four orbital model and that the dπ excited state is doubly degenerate, the transition moment is $M_{CT} = \langle G_{\pm}|m_{\pm}|CT_{\pm}\rangle$ with electronic quantum numbers $m = \pm 4 \rightarrow n = \pm 1$ in the PM approach. According to eq 14 the electronic transition is forbidden since the change in angular momentum $\Delta L_z = n - m = \pm 3$ or ± 5. On the basis of eq 23 and the definitions $M^{VC}{}_{CT} = \langle G_{\pm}|m_{\pm}|CT\rangle$ and $M_{Soret} = \langle G_{\pm}|m_{\pm}|E_{\pm}\rangle$, the transition moment for the CT band is

$$M_{CT}^{VC} = \langle E_{\mp}|\partial V/\partial R|CT\rangle \Delta R M_B \frac{E_{\mp} - E_{CT}}{} = \frac{k\Delta R^2}{2\pi} \frac{\langle e^{\mp in\phi}|\cos(\nu\phi)|e^{\pm i\phi}\rangle}{\Delta E_{CT}} M_B = \frac{k\Delta R^2}{\Delta E_{CT}} \frac{M_B}{2} = \frac{\langle\hbar\omega\rangle_{av}}{\Delta E_{CT}} M_B \quad (23)$$

where $n + 1 = \nu$ for $n = 5$ and $n - 1 = -\nu$ for $n = -5$, i.e., $\nu = \pm 6$. The symmetry of the appropriate vibrational mode corresponds to rhombic distortions of the B_{1g} irreducible representation in the D_{4h} point group normally used for metalloporphyrins. The mixing of the excited states is exactly analogous to the B_{1g} vibronic elements derived for resonance Raman spectroscopy that mix e_{gx}/d_{xz} and e_{gy}/d_{yz} excited states.[53] Since the transition probability is proportional to the square of the transition moment, according to eq 23 we have that $M_{CT}{}^2/M_B{}^2 = (\langle\hbar\omega\rangle_{av}/\Delta E_{CT})^2 \approx (175/10\,000)^2 \approx 3 \times 10^{-4}$ as the ratio of the integrated band intensities, compared to an experimental ratio of integrated intensities $I_{CT}/I_B \approx 7.5 \times 10^{-4}$. The VCPM model predicts that the same terms that give rise to an excited-state splitting in the Soret band (eq 18) must also give rise an excited-state splitting in band III, and this a B_0-term MCD signal for band III. The vibronic B_0-term is given by

$$B_0 = \frac{\langle E_+|L_z|CT\rangle \langle CT|m_{-1}|G_-\rangle \langle G_-|m_{-1}|E_+\rangle}{\Delta E_{CT}} = \frac{\langle E_+|L_z|E_+\rangle \langle E_+|m_{-1}|G_-\rangle^2 \left\langle E_+\left|\frac{\partial V}{\partial R}\right|CT_{\pm}\right\rangle^2}{\Delta E_{CT}{}^2} = \frac{nk^2\Delta R^2}{4\Delta E_{CT}{}^3} M_B{}^2 = n\frac{\langle\hbar\omega\rangle^2 av}{\Delta E_{CT}{}^3} M_B{}^2 \quad (24)$$

Only one of the two possible ground states (a_{1u} or a_{2u}) was used for the calculation. The reason for this is that the band III transition requires orbital overlap provided by the a_{2u} orbital.[8] The a_{1u} orbital has nodes at the pyrrole nitrogens and thus does not contribute. The VCPM model thus accounts for the relative intensity and splitting of band III required to explain the observed B_0-term MCD signal.[8]

Vibronic Approach to the Q-Band Intensity. The VCPM approach also applies to the intensity of the Q-band relative to the Soret band addressed in previous studies.[46] The Q-band transition is forbidden in the PM because the transition moment (eq 14) vanishes for $n \neq m + 1$ for $n, m > 0$ and $n \neq m - 1$ for $n, m < 0$. However, the VCPM introduced above for the vibronically active mode that mixes the Soret and band III excited states can be extended to include intrastate coupling. The vibronic model for the Q-band transition moment is

$$M_Q = \langle G_{\pm}|\mu_{\mp 1}|E_{\pm}\rangle \frac{\langle G_{\mp}|\partial V/\partial R|G_{\pm}\rangle}{\Delta E_Q} \Delta R = \frac{k\Delta R^2}{4\pi^2} \langle e^{\pm in\phi}|e^{\mp i\phi}|e^{\pm im\phi}\rangle \frac{\langle e^{\pm im\phi}|\cos(\nu\phi)|e^{\mp im\phi}\rangle}{\Delta E_Q} = \frac{k\Delta R^2}{\Delta E_Q} \frac{M_B}{4} = \frac{\langle\hbar\omega\rangle_{av}}{\Delta E_Q} M_B \quad (25)$$

where $\Delta E_Q = E_{\pm} - G_{\pm}$.

The Q-band will be allowed if the vibronic mode distorts the ground state. Raman spectra indicate that VC involves one or more high-frequency modes of B_{1g} symmetry that distort the periphery of the porphyrin ring (e.g., ν_{10}, ν_{11}, ν_{13}, etc.) and give rise to H−T coupling of the of π-states of Q- and B-bands.[54,14] In the VCPM approach the vibronic mode must have $\nu = 2n$ (see also Supporting Information). The vibronic distortion in the ground state ($n = 4$) of a mode of A_{2g} symmetry is required for H−T coupling of the Q-band, since $\nu = 8$ (see Figure 7) consistent with the presence of several intense A_{2g} modes in the Q-band resonance Raman spectrum of deoxy hemes.[40,14]

The coupling of a single vibrational mode is not sufficient to explain the Q-band intensity. If we assume that a single 1600 cm^{-1} mode is responsible for the VC and $\Delta E_Q = 16\,000\ cm^{-1}$, then the model predicts that the Q-band is approximately 100 times less intense than the Soret band (i.e., $M_Q{}^2/M_B{}^2 = (\langle\hbar\omega\rangle_{av}/\Delta E_Q)^2 = (1600/16\,000)^2 = 0.01$. The experimentally observed intensity ratios obtained from the integrating the bands in Figures 3−6 are $I_Q/I_B \approx 0.18$ for CO-heme and $I_Q/I_B \approx 0.12$ for deoxy heme. To account for these intensities we can estimate that coupling by four vibronic modes in the same frequency range would give $M_Q \approx 0.4M_B$ and the calculated $I_Q/I_B \approx 0.16$. This is consistent with observation of a number of A_{2g} and B_{1g} modes in the Q-band Raman spectrum. The VCPM model can account for coupling by modes of B_{1g} symmetry if higher order H−T terms are included. This is likely important for deoxy heme where the Q-band has an extended vibronic progression indicative of 0−1 and 0−2 transitions as well as multimode coupling.

Discussion

The PM approach to MCD is computationally and conceptually the most expedient means for estimating the magnitude of spectral shifts and orbital angular momentum quenching due to CT states. For this reason, further development of the technique presented here provides an opportunity to understand MCD spectra in a variety of metalloporphyrins. In addition to vibronic coupling (VC), a key difference between the approach taken here and previous MCD studies is the use of the multiple Gaussian scaled first derivative (MG-SFD) rather than the method of moments (MM) to estimate the MCD effect. As shown in Table 1, the errors in the MG-SFD approach are smaller than those obtained using MM.

The agreement of the VCPM approach with experiment is quite good. According to the PM theory $\Delta L_z = \pm 1$ for the Soret band and $\Delta L_z = \pm 9$ for the Q-band of MbCO giving a ratio $\Delta L_z(Q)/\Delta L_z(B) = 9$. The experimental values for ΔL_z are given in Table 1 for three models. The experimental ratio $\Delta L_z(Q)/\Delta L_z(B) \approx 8.3$ and 6.6 obtained from the MG-SFD method and

MM, respectively. Both the ratio $\Delta L_z(Q)/\Delta L_z(B)$ and the absolute values of ΔL_z are smaller for the method of moments (MM) and scaled first derivative (SFD) methods than for the multiple Gaussian fit with scaled first derivatives (MG-SFD). The reason for this is that MM and SFD give the average of ΔL_z over all of the vibronic bands. The values in Table 1 obtained by the analysis presented in the Supporting Information are consistent with previous work.[24,31] The C_0-term MCD for the deoxy Soret band is in good agreement using the PM theory. The ratio of Q- and B-band angular momentum changes is calculated to be $\Delta L_z(Q)/\Delta L_z(B) = -9/4 = -2.25$ for deoxy Mb, compared to experimental values $\Delta L_z(Q)/\Delta L_z(B) \approx -2.44$ and -2.21 for MG-SFD and MM, respectively. The experimental magnitude of ΔL_z for the Soret band is smaller than that predicted by theory because the C_0-term is temperature-dependent as shown in eq 4.[55]

The MCD signal arises from the change in extinction coefficient due to the interaction of the magnetic field with the difference in angular momentum $\Delta(L_z + 2S_z)$, i.e., a change in the excited-state Zeeman Hamiltonian relative to the ground state. The spin state of the heme iron will not change, i.e., ΔS_z, unless there is strong spin−orbit interaction between the iron and porphyrin ring. While early models of the MCD spectra of open-shell deoxy heme were based on the idea that spin−orbit coupling is large,[23] this assumption has been questioned by other workers.[25,55] An alternative hypothesis developed in this work is that the deoxy ground state consists of nearly degenerate a_{1u} and a_{2u} orbitals, while the deoxy excited state is split by vibronic coupling. This hypothesis does not exclude a role for the spin−orbit interaction; however, it is not necessary and the VCPM approach is a self-consistent treatment. The theory starts with the fact that even in the absence of a strong spin−orbit interaction, there can be mixing of d-orbitals with porphyrin ring orbitals that have the appropriate symmetry.[56] The d_{z^2} orbital mixes with the a_{1u} and a_{2u} ground state and the d_{xz} and d_{yz} orbitals mix with the e_g excited state. Rhombic distortions that explain spectral features in deoxy hemes involve a splitting of the d_π orbitals into d_{xz} and d_{yz}.[55,57] These distortions permit vibronic coupling that splits the excited state of deoxy heme, but not the ground state, leading to a change in ΔL_z when compared to the (unsplit) degenerate excited state. The origin of the Soret band splitting cannot be vibronic interaction with the Q-band transition, since this transition exhibits normal A_1-term MCD, indicative of a degenerate excited state. On the other hand, the VCPM model provides a consistent explanation for the fact that the Soret excited state orbital angular momentum is completely quenched vibronic coupling to band III.[14] The split Soret band observed in low-temperature absorption spectra[17,51] is consistent with Raman,[14,54] magnetization,[55] and Mössbauer data.[57]

The Q-band and band III are vibronically coupled to the Soret band by different vibrational modes of B_{1g} symmetry. Of the nine modes of B_{1g} symmetry, the highest frequency modes (e.g. ν_{10}, ν_{11}, and ν_{13}) involving the periphery of the porphyrin ring are responsible for the coupling of the Q-band to the Soret band. The high-frequency modes involve mostly Cα, Cβ, and Cm carbons of the ring and hence do not couple orbital angular momentum from the iron into the ring. On the other hand, the origin of vibronic coupling of band III involves a rhombic distortion of the Fe−Np bond lengths, i.e., coupling to low-frequency B_{1g} modes. In particular, the 150 cm^{-1} in the band III resonance Raman spectrum and Soret band spectra is involved in the mixing of dπ and $e_g\pi^*$ orbitals. The Raman spectra are consistent with this hypothesis, since a different set of high-frequency modes are resonantly enhanced in Q-band and band III Raman spectra of deoxy heme. The requirement that coupling of a porphyrin $\pi-\pi^*$ transition (Q-band) and charge-transfer transition (band III) to the Soret band must involve different vibronic distortions leads to the consideration of different vibronic matrix elements in VCPM given by eqs 25 and 23 for the Q-band and band III, respectively.

The explanation of the MCD signal for deoxy heme arising from an excited-state splitting due to vibronic coupling to band III is important for the interpretation of a number of experiments in myoglobin biophysics. Nonequilibrium relaxation in myoglobin following photolysis is observed in spectral shifts of the Soret band and band III.[5,15,17−19,21,58−61] The splitting of the Soret and band III excited-state configurations suggests that these band shifts arise from the rhombic distortion along a B_{1g} mode. Symmetry lowering along a nontotally symmetric in-plane normal coordinate provides an alternative hypothesis to the current interpretation of spectral shifts in myoglobin. One hypothesis holds that electronic band shifts are coupled to the iron axial out-of-plane displacement.[5,15,17,18,21,58,59,61] The MCD and resonance Raman data suggest an alternative hypothesis, that protein structural rearrangements around the photolyzed ligand (e.g., CO in Mb*CO) induce geometry distortions of the heme that would account for the splitting of the Soret band. The coupling to band III is an intrinsic property of deoxy hemes and the observations proposed here can be tested in a range of heme proteins and model systems.

The application of MCD to open-shell systems has lacked simple theoretical approaches. Koboyashi developed models to account for the admixture of charge-transfer states of open-shell metals with the porphyrin ring (see Supporting Information).[29,33,34] The mixing of charge transfer states can account for the effective quenching of orbital angular momentum in metaquo Mb where $\Delta L_z \approx 0.25$ for the Soret band and $\Delta L_z \approx 4$ for the Q-band based on MCD spectra (metaquo data not shown). Koboyashi's model does not apply to deoxy ferrous heme, since that model can only account for quenching of the orbital angular momentum and not vibronic coupling that would lead to a splitting of the excited state. The MCD signal in deoxy heme indicates nearly complete elimination of the orbital angular momentum of the Soret excited state. A combination of the vibronic approach and Koboyashi's approach will have application to both ferric and ferrous heme MCD spectra. There is presently a wealth of MCD spectra available that contain quantitative information regarding the spin state, admixture of charge-transfer states, and splitting of the ground and excited states. Thus, the approach here provides a general approach to a simple interpretation of heme MCD spectra.

Acknowledgment. S.F. gratefully acknowledges support by NSF-CAREER award (MCB-9874895). S.F. thanks Dr. John Dawson of the University of South Carolina for use of equipment to obtain magnetic circular dichroism spectra and Dr. Mark Roach for assistance in the data collection.

Supporting Information Available: Discussion that connects the perimeter model proposed to earlier work and a comparison of the data analysis by three methods: (1) the method of moments; (2) the derivative method, which includes a scaled derivative method and multiple Gaussian band fitting; (3) the rigid shift Gaussian method. This material is available free of charge via the Internet at http://pubs.acs.org.

References and Notes

(1) Stephens, P. J.; Suetaak, W.; Schatz, P. N. *J. Chem. Phys.* **1966**, *44*, 4592−4602.

(2) Jones, R.; Jayaraj, K.; Gold, A.; Kirk, M. L. *Inorg. Chem.* **1998**, *37*, 2842−2843.

(3) Austin, R. H.; Beeson, K. W.; Eisenstein, L.; Frauenfelder, H.; Gunsalus, I. C. *Biochemistry* **1975**, *14*, 5355−5373.

(4) Lambright, D. G.; Varadarajan, R.; Boxer, S. G. *J. Mol. Biol.* **1989**, *207*, 289−299.

(5) Lim, M.; Jackson, T. A.; Anfinrud, P. A. *Proc. Natl. Acad. Sci. U. S. A.* **1993**, *90*, 5801−5804.

(6) Tian, W. D.; Sage, J. T.; Srajer, V.; Champion, P. M. *Phys. Rev. Lett.* **1992**, *68*, 408−411.

(7) Zerner, M.; Gouterman, M.; Kobayashi, H. *Theor. Chim. Acta* **1966**, *6*, 363−400.

(8) Eaton, W. A.; Hanson, L. K.; Stephens, P. J.; Sutherland, J. C.; Dunn, J. B. R. *J. Am. Chem. Soc.* **1978**, *100*, 4991−5003.

(9) Andrews, B. K.; Romo, T.; Clarage, J. B.; Pettitt, B. M.; Phillips, G. N. *Struct. Folding Design* **1998**, *6*, 587−594.

(10) Olson, J. S.; Phillips, G. N., Jr. *J. Biol. Inorg. Chem.* **1997**, *2*, 544−552.

(11) Schlichting, I.; Berendzen, J.; Phillips, G. N., Jr.; Sweet, R. M. *Nature* **1994**, *371*, 808−812.

(12) Hartmann, H.; Zinser, S.; Komninos, P.; Schneider, R. T.; Nienhaus, G. U.; Parak, F. *Proc. Natl. Acad. Sci. U. S. A.* **1996**, *93*, 7013−7016.

(13) Srajer, V.; Teng, T. Y.; Ursby, T.; Pradervand, C.; Ren, Z.; Adachi, S.; Schildkamp, W.; Bourgeois, D.; Wulff, M.; Moffat, K. *Science* **1996**, *274*, 1726−1729.

(14) Franzen, S.; Wallace-Williams, S. E.; Shreve, A. P. *J. Am. Chem. Soc.*, in press.

(15) Jackson, T. A.; Lim, M.; Anfinrud, P. A. *Chem. Phys.* **1994**, *180*, 131−140.

(16) Huang, J.; Ridsdale, A.; Wang, J. Q.; Friedman, J. M. *Biochemistry* **1997**, *36*, 14353−14365.

(17) Srajer, V.; Champion, P. M. *Biochemistry* **1991**, *30*, 7390−7402.

(18) Steinbach, P. J.; Ansari, A.; Berendzen, J.; Braunstein, D.; Chu, K.; Cowen, B. R.; Ehrenstein, D.; Frauenfelder, H.; Johnson, J. B.; Lamb, D. C.; Luck, S.; Mourant, J. R.; Nienhaus, G. U.; Ormos, P.; Philipp, R.; Xie, A.; Young, R. D. *Biochemistry* **1991**, *30*, 3988−4001.

(19) Franzen, S.; Boxer, S. G. *J. Biol. Chem.* **1997**, *272*, 9655−9660.

(20) Schulze, B. G.; Grubmuller, H.; Evanseck, J. D. *J. Am. Chem. Soc.* **2000**, *122*, 8700−8711.

(21) Gilch, H.; SchweitzerStenner, R.; Dreybrodt, W.; Leone, M.; Cupane, A.; Cordone, L. *Int. J. Quantum Chem.* **1996**, *59*, 301−313.

(22) Livshitz, M. A.; Arutyunyan, A. M.; Sharonov, Y. A. *J. Chem. Phys.* **1976**, *64*, 1276−1280.

(23) Treu, J. I.; Hopfield, J. J. *J. Chem. Phys.* **1975**, *63*, 613−623.

(24) Malley, M.; Feher, G. *J. Mol. Spec.* **1968,** *26*, 320−334.

(25) Seno, Y.; Kameda, N.; Otsuka, J. *J. Chem. Phys.* **1980**, *72*, 6059−6069.

(26) Platt, J. R. *J. Chem. Phys.* **1949**, *17*, 484−495.

(27) Simpson, W. T. J. *J. Chem. Phys.* **1949**, *17*, 1218−1221.

(28) Kuhn, H. J. *J. Chem. Phys.* **1949**, *17*, 1198−1212.

(29) Koboyashi, H. *J. Chem. Phys.* **1959**, *30*, 1361−1362.

(30) Longuet-Higgins, H. C.; Rector, C. W.; Platt, J. R. *J. Chem. Phys.* **1950**, *18*, 1174−1181.

(31) Michl, J. *J. Am. Chem. Soc.* **1978**, *100*, 6812−6818.

(32) Michl, J. *J. Am. Chem. Soc.* **1978**, *100*, 6801−6811.

(33) Koboyashi, H.; Shimizu, M.; Fujita, I. *Bull. Chem. Soc. Jpn.* **1970**, *43*, 2335−2341.

(34) Koboyashi, H.; Higuchi, T.; Eguchi, K. *Bull. Chem. Soc. Jpn.* **1976**, *49*, 457−463.

(35) Shelnutt, J. A. *J. Chem. Phys.* **1981**, *74*, 6644−6657.

(36) Callahan, P. M.; Babcock, G. T. *BIOCHEMISTRY* **1981**, *20*, 952−958.

(37) Parthasarathi, N.; Hansen, C.; Yamaguchi, S.; Spiro, T. G. *J. Am. Chem. Soc.* **1987**, *109*, 3865−3871.

(38) Friedman, J. M.; Rousseau, D. L.; Ondrias, M. R. *Annu. Rev. Phys. Chem.* **1982**, *33*, 471−491.

(39) Stein, P.; Terner, J.; Spiro, T. G. *J. Phys. Chem.* **1982,** *86*, 168−170.

(40) Spiro, T. G.; Strekas, T. C. *Proc. Natl. Acad. Sci.* **1972**, *69*, 2622−2626.

(41) Rosenfeld, Y. B.; Stavrov, S. S. *Chem. Phys. Lett.* **1994**, *229*, 457−464.

(42) Stephens, P. J. *J. Chem. Phys.* **1970**, *52*, 3489−3516.

(43) Sutherland, J. C.; Axelrod, D.; Klein, M. P. *J. Chem. Phys.* **1971**, *54*, 2888−2898.

(44) Fuhrhop, J.-H.; Smith, K. M. In *Porphyrins and Metalloporphyrins*; Smith, K. M., Ed.; Elsevier: Amsterdam, 1975; pp 804−807.

(45) Dawson, J. H.; Kadkhodayan, S.; Zhuang, C.; Sono, M. *J. Inorg. Biochem.* **1992**, *45*, 179−192.

(46) Perrin, M. H.; Gouterman, M.; Perrin, C. L. *J. Chem. Phys.* **1969**, *50*, 4137−4150.

(47) Piepho, S. B.; Schatz, P. N. *Group Theory in Spectroscopy with Application to Magnetic Circular Dichroism*; John Wiley & Sons: New York, 1983.

(48) Liptay, W. *Ber. Bunsen.* **1976**, *80*, 207−217.

(49) Mathies, R.; Albrecht, A. C. *J. Phys. Chem.* **1974**, *60*, 2500−2508.

(50) Bublitz, G. U.; Boxer, S. G. *Annu. Rev. Phys. Chem.* **1997**, *48*, 213−242.

(51) Franzen, S.; Morre, L. J.; Woodruff, W. H.; Boxer, S. G. *J. Am. Chem. Soc.* **1981**, *103*, 3070−3072.

(52) Vickery, L.; Nozawa, T.; Sauer, K. *J. Am. Chem. Soc.* **1975**, *98*, 343−350.

(53) Shelnutt, J. A.; Cheung, L. D.; Chang, R. C. C.; Yu, N. T.; Felton, R. H. *J. Chem. Phys.* **1977**, *66*, 3387−3396.

(54) Bangcharoenpaurpong, O.; Schomaker, K. T.; Champion, P. M. *J. Am. Chem. Soc.* **1984**, *106*, 5688−5698.

(55) Oganesyan, V. S.; Sharonov, Y. A. *Spectrochim. Acta A* **1997**, *53*, 433−449.

(56) Shelnutt, J. A.; O'Shea, D. C.; Yu, N.-T.; Cheung, L. D.; Felton, R. H. *J. Chem. Phys.* **1976**, *64*, 1156−1165.

(57) Eicher, H.; Bade, D.; Parak, F. *J. Chem. Phys.* **1976**, *64*, 1446−1455.

(58) Kiger, L.; Stetzkowski-Marden, F.; Poyart, C.; Marden, M. *Eur. J. Biochem.* **1995**, *228*, 665−668.

(59) Chavez, M. D.; Courtney, S. H.; Chance, M. R.; Kuila, D.; Nocek, J.; Hoffman, B. M.; Friedman, J. M.; Ondrias, M. R. *Biochemistry* **1990**, *29*, 4844−4852.

(60) Lambright, D. G.; Balasubramanian, S.; Boxer, S. G. *Biochemistry* **1993**, *32*, 10116−10124.

(61) Ansari, A.; Jones, C. M.; Henry, E. R.; Hofrichter, J.; Eaton, W. A. *Biochemistry* **1994**, *33*, 5128−5145.